

Calculations of electron-impact excitation and dielectronic recombination rate coefficients of highly charged silicon ions

L. Y. Xie^{1,*}, J. L. Rui¹, J. M. Zhang¹, R. Schuch², and C. Z. Dong^{1,†}

¹Key Laboratory of Atomic and Molecular Physics and Functional Materials of Gansu Province, College of Physics and Electronic Engineering, Northwest Normal University, Lanzhou 730070, People's Republic of China

²Department of Physics, Stockholm University, AlbaNova University Center, SE-10691 Stockholm, Sweden



(Received 10 August 2021; accepted 7 January 2022; published 31 January 2022)

The rate coefficients for dielectronic recombination and electron-impact excitation processes with H-like to Be-like silicon ions (Si^{13+} - Si^{10+}) are calculated using relativistic distorted-wave approach. The prominent $\Delta n = 1$ and the weaker $\Delta n = 2$ and 3 dielectronic recombination (DR) resonances with K -shell excitations are presented, and compared with the existing DR experimental rate coefficients of Si^{13+} , Si^{12+} , and Si^{11+} ions, it is found that the theoretical DR rate coefficients are in very good agreement with the experimental results. With the same approach, the direct and resonant electron-impact excitation (EIE) cross sections associated with $1s - n'l'$ core excitations are calculated for the ground states of Si^{13+} - Si^{10+} ions and found in excellent agreement with the available experiment. Finally, we present the synthesized DR and EIE rate coefficients for the sum of all detected ($13+ \sim 10+$) charge states of Si and these agree well with the experimental results.

DOI: [10.1103/PhysRevA.105.012823](https://doi.org/10.1103/PhysRevA.105.012823)

I. INTRODUCTION

Collisions of electron with highly charged ions (HCIs) are of fundamental interest, and are among the most important processes in astrophysical and laboratory plasma [1]. In these collisions electrons might recombine with ions through different reactions. Dielectronic recombination (DR) is a resonant electron-ion recombination process, in which a free electron is captured into the HCI with the simultaneous excitation of a bound electron, thus forming an intermediate double excited state that is stabilized by decaying radiatively to an energetically lower state [1–3]. Since DR changes the charge state of ions, it strongly affects both the charge-state distribution and the emitted x-ray spectrum [2,3]. On the other hand, if the double excited state decays by autoionization the ion returns back to its original charge state. This process is called resonant excitation (RE). Besides that occurs also nonresonant or “direct” excitation (DE). The impacting electron loses energy by exciting the ion which stabilizes by photon emission [1]. Electron-impact excitation (EIE) processes occur usually at higher electron energies than DR, and will significantly influence the electron-impact reaction rates and line emission intensities of the HCIs. Therefore, accurate knowledge of DR and EIE cross sections and rate coefficients are needed for modeling of astrophysical and fusion plasmas [1–4].

Highly charged silicon ions widely exist in high-temperature astrophysical and laboratory plasmas [1–4]. Silicon is an important element in the solar system. Consequently, prominent photoemission lines from silicon

ions are observed in solar emission and absorption spectra such as from the solar corona [5,6]. Observations of emission and absorption lines of various charge states of silicon range from hot astrophysical objects to the intergalactic medium such as stellar atmospheres [7], Doppler imaging analysis of star atmospheres; star abundances [8], supernova remnants [9,10], active galactic nuclei [11], quasars with high redshifted lines [12] and black hole, neutron star physics and binaries studied by Doppler spectroscopy [13]. Thus, accurate atomic data of silicon ions are required in order to identify spectral lines, derive ion abundances, and carry out plasma diagnostics.

After the pioneering work of Burgess [2], it took around 20 years until the first experimental studies of the DR process have been performed. Then, in the end of the 1980s the advent of heavy-ion cooler storage rings [14] and electron beam ion traps (EBIT) [15] caused a revolutionary development in electron-ion collision experiments. These devices allow investigations of reactions between electrons and ions in almost any charge state with high resolution and luminosity and signal-to-background ratio [16].

In the literature there are now several experimental results of DR rate coefficients for highly charged silicon ions in various charge states [17–22]. But comparably few systematic studies for the EIE process with highly charged ions over the whole nuclear charge range (see, e.g., Refs. [23–26]) were done, almost all of them at EBITs, where the combined DR and EIE processes are detectable in the photon spectra and by discrimination in the photon energy, EIE is identified [23,25,26].

Recently, Lindroth *et al.* [27] reported measurements of electron-impact recombination and excitation rates of charge-state-selected H-like Si^{13+} to Be-like Si^{10+} ions at the Stockholm electron beam ion trap. We shall try to model

*xiely@nwnu.edu.cn

†dongcz@nwnu.edu.cn

the experimental spectra of Ref. [27], in order to test our theoretical model and to identify the important DR and EIE reaction channels.

In this work, we follow the analysis done in Ref. [28] and give first an account of the calculations of the electron-ion recombination rate coefficients, and DE and RE rate coefficients using the flexible atomic code (FAC) [29] based on a relativistic configuration interaction (RCI) method. In Sec. III, the theoretical calculations of DR and EIE rate coefficients are presented, followed by a comparison with the experimental results.

II. THEORETICAL METHODS

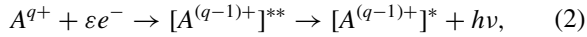
In general, for a particular electron-impact process, such as DR or EIE, the rate coefficients are related to the corresponding cross sections as follows:

$$\alpha(\varepsilon_e) = \int \sigma v f(v) dv, \quad (1)$$

where ε_e is the kinetic energy, v is the velocity of the impacting electrons, and $f(v)$ denotes the Gaussian resolution function (mainly the velocity distribution of the electron beam in EBIT [27]). The integration over v runs from 0 to infinity ($+\infty$).

A. Dielectronic recombination

As stated above, the DR process can be formulated as



where A^{q+} denotes the initial target ion (i), $[A^{(q-1)+}]^{**}$ is the resonant doubly excited state (d), and $[A^{(q-1)+}]^{*}$ is the recombined ion after the radiative decay process (f), in any bound state which is energetically below its autoionization threshold. In the isolated resonance approximation [30], the DR cross section can be well approximated by a Lorentz resonance profile $L(\varepsilon_e) = \frac{\Gamma/2\pi}{(E_{id}-\varepsilon_e)^2 + \Gamma^2/4}$ and a strength S_d as a function of the electron energy ε_e as follows:

$$\sigma(\varepsilon_e) = S_d L_d(\varepsilon_e). \quad (3)$$

In this approximation, the natural width Γ of the doubly excited state d has been assumed to be much smaller than the spread of the electron energy ε_e and the energy separation from neighboring resonances. E_{id} denotes the energy separation of the doubly excited state d from the initial state i , i.e., the DR resonance energy. The integrated DR cross section, that is, the DR strength S_d for a given double excited d , is proportional to the autoionization rate $A^a(d - i)$ to i times the radiative branching ratio $B(d)$ to all radiative final states f [1] (atomic units are used throughout unless specified),

$$S_d = \frac{g_d \pi^2}{2 g_i E_{id}} A^a(d \rightarrow i) B(d), \quad (4)$$

where g_i and g_d are the statistical weights of the states i and d , respectively. The branching ratio for DR through the level

d is

$$B(d) = \frac{\sum_f A^r(d \rightarrow f)}{\sum_k A^a(d \rightarrow k) + \sum_f A^r(d \rightarrow f)}, \quad (5)$$

where A^a and A^r denote the autoionization and radiative decay rates, respectively. In the sums, k denotes all excited states which are attainable by autoionization of the state d , and f runs over all radiative final states which lie below d . For HCIs, the DAC effect on DR strength is usually so small [29,31] that it can be ignored in the present calculations.

The radiative decay rate A^r is given by

$$A^r = \frac{4\omega_p^3}{3c^3 g_d} |\langle \psi_f | T^{(t)} | \psi_d \rangle|^2, \quad (6)$$

where ψ_d and ψ_f are atomic-state functions (ASFs) for the states d and f , respectively, c is the speed of light, and ω_p is the frequency of the decay photons. $T^{(t)}$ denotes the multipole radiative tensor operator. The autoionization (Auger) decay rate can be given by

$$A^a = 2 \sum_{\kappa} |\langle \psi_i, \kappa; J_T M_T | V_{ee} | \psi_d \rangle|^2; \quad (7)$$

similarly, ψ_i represents the ASF of the combined system “the initial target ion plus the impacting electron.” κ is the relativistic angular quantum number of the free electron, V_{ee} denotes the usual electron-electron interaction operator, which consists of the Coulomb and Breit operators, and is given by

$$V_{ee} = \sum_{p < q} (V_{\text{Coul}} + V_{\text{Breit}}), \quad (8)$$

where $V_{\text{Coul}} = \frac{1}{r_{pq}}$ denotes the Coulomb operator, and V_{Breit} is the Breit operator [32,33].

To compare the theoretical calculations with the EBIT experimental results, each of the individual DR resonance strengths S_d is subsequently convoluted with the resolution function, which is here approximated by a $\Delta E = 18$ -eV-wide (FWHM) Gaussian distribution [27]. The total DR cross section σ_i^{DR} from the level i can be obtained by summing over all intermediate resonant states d [31]:

$$\sigma_i^{\text{DR}}(\varepsilon_e) = \sum_d \frac{2}{\Delta E} \left(\frac{\ln 2}{\pi} \right)^{1/2} \exp \left[-4 \ln 2 \left(\frac{\varepsilon_e - E_{id}}{\Delta E} \right)^2 \right] S_d. \quad (9)$$

B. Electron-impact excitation

In the isolated resonance approximation, total EIE cross section from an initial state i to an excited final state f consists of DE and RE contributions

$$\sigma_{\varepsilon_e}^{\text{EIE}}(i \rightarrow f) = \sigma_{\varepsilon_e}^{\text{DE}}(i \rightarrow f) + \sigma_{\varepsilon_e}^{\text{RE}}(i \rightarrow f), \quad (10)$$

where interference effects between the DE and RE are neglected. The DE cross section can be expressed in terms of the collision strength

$$\sigma_{\varepsilon_e}^{\text{DE}}(i \rightarrow f) = \frac{\pi}{k_e^2 g_i} \Omega_{\varepsilon_e}^{\text{DE}}(i \rightarrow f) \quad (11)$$

in this expression k_e is the relativistic wave number of the impacting electron [34]

$$k_e^2 = 2\varepsilon_e \left[1 + \frac{\alpha^2}{4} \varepsilon_e \right], \quad (12)$$

where α is the fine-structure constant.

The collision strength $\Omega_{\varepsilon_e}^{\text{DE}}(i - f)$ can be expressed as [29]

$$\begin{aligned} \Omega_{\varepsilon_e}^{\text{DE}}(i - f) &= 2 \sum_{\kappa_i \kappa_f} \sum_{J_T} (2J_T + 1) |\langle \psi_i \kappa_i, J_T M_T | \\ &\quad \times \sum_{i < j} \frac{1}{r_{ij}} |\psi_f \kappa_f, J_T M_T \rangle|^2, \end{aligned} \quad (13)$$

where κ_i and κ_f are the relativistic angular quantum numbers of the incident and scattered electrons, respectively. J_T is the total angular momentum when the target state is coupled to the continuum orbital, and M_T is the projection of the total angular momentum. The RE process can be treated as a two-step process, i.e., resonant electron capture by an N -electron ion in the initial state i to form a $(N + 1)$ -electron resonant excited state d followed by autoionization to the final state f . With such a theoretical treatment, the resonance excitation cross section $\sigma_{\varepsilon_e}^{\text{RE}}(i \rightarrow f)$ is given by [23,35]

$$\sigma_{\varepsilon_e}^{\text{RE}}(i \rightarrow f) = \frac{g_d \pi^2}{2g_i E_{id}} \sum_d A^a(d \rightarrow i) B(d \rightarrow f) L(\varepsilon_e). \quad (14)$$

In this equation, $B(d \rightarrow f)$ represents the autoionization branching ratio and is expressed as

$$B(d \rightarrow f) = \frac{A^a(d \rightarrow f)}{\sum_m A^a(d \rightarrow m) + \sum_{m'} A^r(d \rightarrow m')}, \quad (15)$$

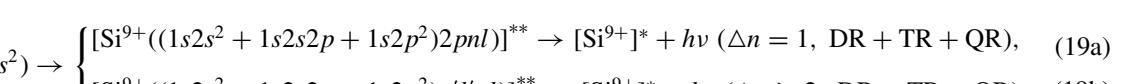
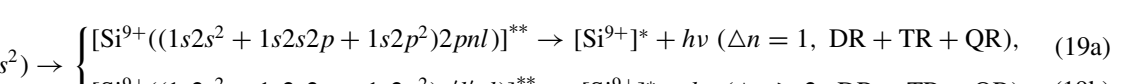
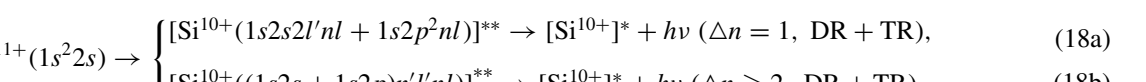
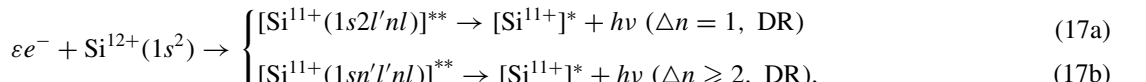
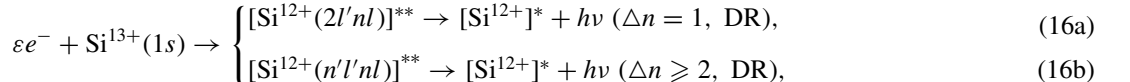
where the radiative decay rate A^r and the autoionization rate A^a are given by Eqs. (6) and (7), respectively.

As seen from Eqs. (1), (3), and (10), the calculations of the rate coefficients can be traced back to evaluate the DR resonance energies, EIE excitation energies, and collision strengths as well as the radiative and autoionization decay rates.

III. RESULTS AND DISCUSSION

A. DR rate coefficients

In this study, we employed the FAC [29] to calculate the electronic structure of $\text{Si}^{13+} \sim \text{Si}^{10+}$ ions, and a relativistic distorted-wave approximation to describe the continuum states. In the calculation of wave functions and energy levels for the initial, intermediate resonance states and the radiative final states, the contributions from electron correlations, quantum electrodynamics (QED), and Breit interaction were considered. First, the following DR processes of $\text{Si}^{13+} \sim \text{Si}^{10+}$ ions have been studied:



For H-like $\text{Si}^{13+}(1s)$ and He-like $\text{Si}^{12+}(1s^2)$ ions, we considered the dominant DR channels as shown in Eqs. (16) and (17), respectively. Taking the $\text{Si}^{13+}(1s^2S_{1/2})$ in the ground state as an example, Eqs. (16a) and (16b) describe the inner K -shell resonant states in the $\Delta n = 1$ and $\Delta n \geq 2$ DR processes. Here and below, n' and l' denote the principal quantum number and orbital angular momentum number, respectively, of the electron excited in the parent ion upon recombination (core excited electron), and nl are the analogous quantum numbers of the captured (Rydberg) electron. For DR a distinction is made whether the core electron is excited to the next higher shell ($1s \rightarrow 2l'$) ($\Delta n = 1$ DR) or it is excited to a higher shell ($1s \rightarrow n'l'$) ($\Delta n \geq 2$ DR). The $n' = 3-4$, maximum Δn up to 3, and n up to 30 are included

in our calculations. The same way was used for the other silicon ions. Both DR and trielectronic recombination (TR) [36] channels are incorporated for Li-like $\text{Si}^{11+}(1s^22s)$ ions due to complex electron correlations. The quadruelectronic recombination (QR) [37] channels are further added for Be-like $\text{Si}^{10+}(1s^22s^2)$ ions. In this work, we carried out the detailed level-by-level computations including configuration mixing between the DR, TR, and QR resonance states as described above. It is found that those configuration mixings influence the total DR strengths or cross sections up to about 12%, and have very small effects on resonance energies of H-like to Be-like silicon ions. For $\Delta n = 1$ DR processes as an example, when the TR channels were included in the calculations, it reduced the total strength of Li-like Si^{11+} ions considering

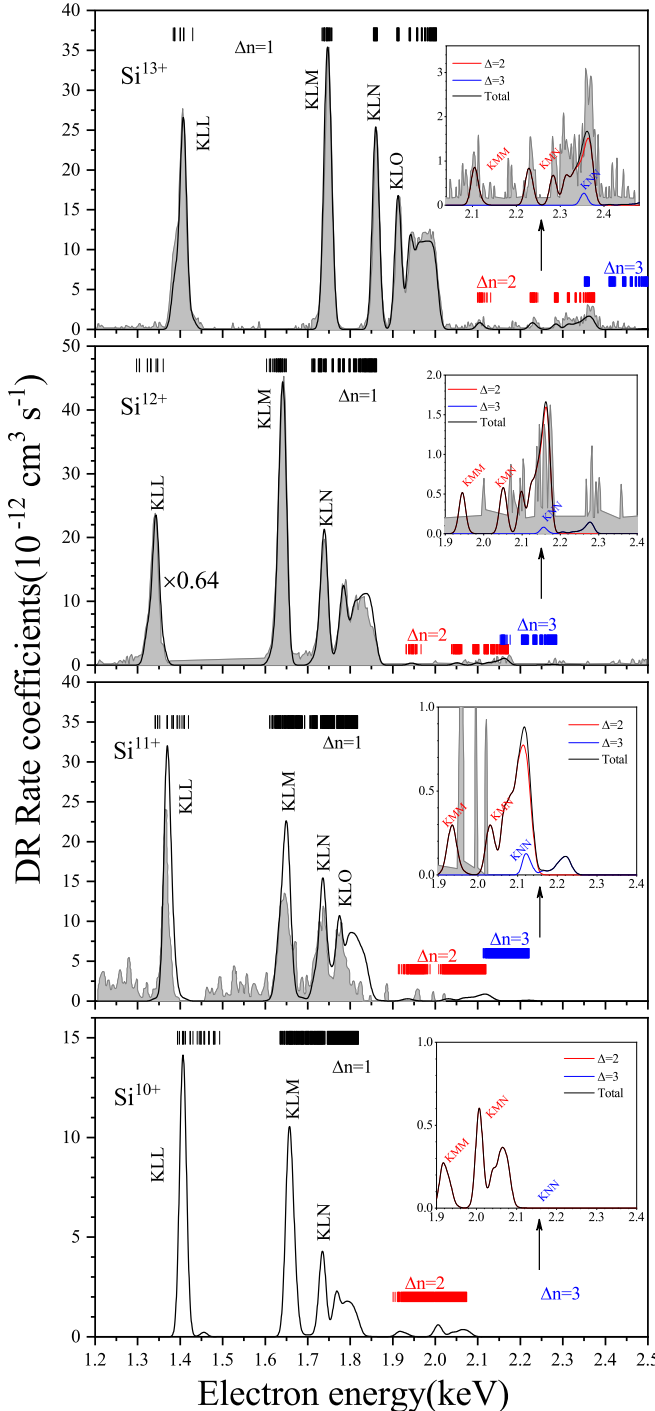


FIG. 1. The calculated total electron-ion recombination rate coefficients (black curves) of H-like to Be-like silicon ions in the ground states compared with the EBIT measurements (gray area) [27]. Inset: Partial enlarged detail. The red and blue curves indicate theoretical recombination rate coefficients for $\Delta n = 2$ and 3 DR processes, respectively. The colored vertical bars show the resonance positions for each of the individual resonances.

only the DR channel by 2.11%. For Be-like Si^{10+} ions, when the TR and QR channels were further included, the total DR strength was reduced by 12.24%.

In Fig. 1, the theoretical results of the total electron-ion recombination rate coefficients of Si^{13+} , Si^{12+} , Si^{11+} , and

Si^{10+} ions in the ground states are presented, and compared with the EBIT measurements by Lindroth *et al.* [27]. The DR resonances located at lower resonant energy regions associated with $\Delta n = 1(1s - 2l)$ excitation show a series of strong peaks identified by the standard notations KLL , KLM , KLN , and KLO . Each of the resonant peaks contains a number of individual resonances. Their resonance energy positions are shown as colored vertical bars in the figure, and are also listed together with the resonance strengths in Tables I and II for KLL and KLM manifolds, respectively. From the data given in the tables, we find that our calculated resonant energies agree well with available theoretical calculations using MCDF and RCI method by Baumann *et al.* [21], and the experimental values from the NIST database [38], with a deviation less than 0.44% for H-like to Be-like silicon ions. The difference of resonance strength between our results and the theoretical results of Baumann *et al.* [21] are within 10% for most of the stronger resonances with $S_d > 10^{-20} \text{ cm}^2 \text{ eV}$. However, for weaker resonances, such as $((1s_{1/2}2p_{1/2})_12p_{3/2})_{5/2}$ of Si^{10+} ions which $E_{id} = 1478.4 \text{ eV}$, $S_d = 4.61 \times 10^{-24} \text{ cm}^2 \text{ eV}$, there are larger differences of around 46% existing. In Tables I and II, we identified the excitation types including DR, TR, and QR processes. There it can be seen that the TR contributions are important, that is, 0.79% and 1.59% to the total strength of Si^{11+} and Si^{10+} ions, respectively. Furthermore, the QR contribution is 0.07% for Si^{10+} in KLL manifolds. In KLM manifolds, the TR contributions are 3.35% and 2.50% for Si^{11+} and Si^{10+} ions, respectively. The QR contribution is 0.11% for Si^{10+} ions. Compared to the $\Delta n = 1$ resonances, the recombination rate coefficients of $\Delta n = 2$ and 3 DR process are rather weak, and decrease rapidly with increasing Δn .

Comparisons are made between our calculated DR rate coefficient and the EBIT experimental values [27]. It is found that the theoretical results of H-like Si^{13+} ions agree very well with the experimental results. For He-like Si^{12+} ions, the theoretical results are multiplied by a factor of 0.64 to make them consistent with the measured results [27]. For Li-like Si^{11+} ions, there are some differences existing between our calculated recombination rate coefficients and the measured values (see Fig. 1). It should be noted, however, that the Li-like DR data of Ref. [27] have larger statistical and systematic error bars than the H- and He-like data. To explore such differences for Li-like Si^{11+} ions further, Fig. 2 plotted the theoretical cross sections folded with the experimental energy resolution of 7 eV (FWHM), and compared with the measured absolute cross sections by Kenntner *et al.* [17] at the Heidelberg heavy-ion storage ring TSR. The theoretical results agree well with the experiment [17] for KLn , $n > 3$, Rydberg series of DR resonances, and also for $\Delta n = 2(1s - 3l)$ series located at higher energies above 1860 eV. It should be noted that the KLL resonant peaks have not been observed in the experiment, and the KLM peaks are about 20% lower than theory.

In Fig. 3, the synthesized $\Delta n = 1$, 2, and 3 recombination rate coefficients of Si^{13+} , Si^{12+} , Si^{11+} , and Si^{10+} ions are shown, together with the experimental measurements by Lindroth *et al.* [27]. It can be clearly seen that the theoretical results are in very good agreement with the experimental

TABLE I. (*Continued.*)

Ions	Resonance states	Type	Resonance energies			Resonance strengths			
			This	NIST [38]	MCDF [21]	FAC [21]	This	MCDF [21]	FAC [21]
Si^{10+}	$(1s_{1/2}2p_{3/2})_1$	TR	1419.5	1416.0	1418.9	1419.4	2.91(-23)	6.29(-23)	6.72(-24)
	$(1s_{1/2}2s_{1/2}^22p_{1/2})_{1/2}$	DR	1393.7		1391.5	1395.2	7.86(-25)	2.71(-22)	1.17(-24)
	$((1s_{1/2}2s_{1/2}^22p_{1/2})_02p_{3/2})_{3/2}$	DR	1393.9		1391.9	1395.6	1.01(-25)	5.55(-23)	7.68(-22)
	$(1s_{1/2}2s_{1/2}^22p_{3/2})_{5/2}$	DR	1394.4		1392.3	1396.1	5.13(-24)	1.65(-21)	4.56(-24)
	$((1s_{1/2}2s_{1/2})_12p_{1/2})_{1/2}2p_{3/2})_{5/2}$	TR	1398.5				3.52(-30)		
	$((1s_{1/2}2s_{1/2})_12p_{1/2})(2p_{3/2})_{5/2}$	DR	1405.7		1403.6	1407.5	6.14(-20)	1.48(-19)	6.19(-20)
	$((1s_{1/2}2s_{1/2})_02p_{3/2})_{3/2}$	DR	1405.8		1403.7	1407.6	4.25(-20)	1.03(-19)	4.26(-20)
	$((1s_{1/2}2s_{1/2})_02p_{1/2})(2p_{3/2})_{1/2}$	DR	1408.0		1405.8	1410.1	1.23(-21)	4.71(-21)	2.44(-21)
	$(1s_{1/2}2s_{1/2}^22p_{3/2})_{3/2}$	DR	1408.9		1406.7	1411.0	4.94(-21)	1.74(-20)	3.73(-21)
	$(1s_{1/2}2s_{1/2}^22p_{3/2})_{1/2}$	DR	1412.6		1409.7	1413.7	1.71(-20)	4.44(-20)	1.93(-20)
	$((1s_{1/2}2s_{1/2})_12p_{1/2})_{3/2}2p_{3/2})_{7/2}$	TR	1422.8				5.16(-29)		
	$((1s_{1/2}2s_{1/2})_12p_{1/2})_{1/2}2p_{3/2})_{5/2}$	TR	1423.0				1.25(-28)		
	$((1s_{1/2}2s_{1/2})_12p_{1/2})_{1/2}2p_{3/2})_{3/2}$	TR	1423.1				1.62(-25)		
	$((1s_{1/2}2s_{1/2})_12p_{1/2})_{3/2}2p_{3/2})_{1/2}$	TR	1423.1				1.46(-25)		
	$((1s_{1/2}2s_{1/2})_02p_{1/2})_{1/2}2p_{3/2})_{3/2}$	TR	1424.4				1.32(-24)		
	$((1s_{1/2}2s_{1/2})_12p_{1/2})_{3/2}2p_{3/2})_{3/2}$	TR	1430.1				2.05(-25)		
	$((1s_{1/2}2s_{1/2})_12p_{3/2})_{5/2}$	TR	1430.1				1.06(-26)		
	$((1s_{1/2}2s_{1/2})_12p_{1/2})_{1/2}2p_{3/2})_{1/2}$	TR	1430.1				1.51(-25)		
	$((1s_{1/2}2s_{1/2})_02p_{1/2})_{1/2}2p_{3/2})_{3/2}$	TR	1439.8				5.39(-24)		
	$((1s_{1/2}2s_{1/2})_02p_{1/2})_{1/2}2p_{3/2})_{5/2}$	TR	1439.9				1.88(-27)		
	$((1s_{1/2}2s_{1/2})_02p_{1/2})_{1/2}2p_{3/2})_{3/2}$	TR	1444.9				7.00(-25)		
	$((1s_{1/2}2s_{1/2})_02p_{1/2})_{1/2}2p_{3/2})_{1/2}$	TR	1446.9				9.43(-23)		
	$((1s_{1/2}2s_{1/2})_02p_{1/2})_{0}2p_{1/2}^22p_{3/2})_{3/2}$	TR	1446.9				1.45(-22)		
	$((1s_{1/2}2s_{1/2})_02p_{1/2})_{1/2}2p_{3/2})_{5/2}$	TR	1449.0				3.41(-29)		
	$((1s_{1/2}2s_{1/2})_12p_{1/2})_{1/2}2p_{3/2})_{3/2}$	TR	1449.3				4.95(-25)		
	$((1s_{1/2}2s_{1/2})_12p_{1/2})_{1/2}2p_{3/2})_{1/2}$	TR	1456.1				5.68(-22)		
	$((1s_{1/2}2s_{1/2})_02p_{3/2})_{3/2}$	TR	1456.2				9.00(-22)		
	$((1s_{1/2}2s_{1/2})_12p_{1/2})_{3/2}2p_{3/2})_{1/2}$	TR	1457.5				3.37(-22)		
	$(1s_{1/2}2p_{1/2}^22p_{3/2})_{5/2}$	QR	1467.2		1461.6	1465.8	5.14(-26)	8.49(-23)	6.07(-26)
	$((1s_{1/2}2p_{1/2})_02p_{3/2})_{3/2}$	QR	1467.9		1462.3	1466.6	6.64(-27)	1.93(-23)	1.05(-26)
	$(1s_{1/2}2p_{3/2})_{1/2}$	QR	1468.3		1462.6	1466.9	1.38(-25)	1.60(-23)	1.58(-25)
	$((1s_{1/2}2p_{1/2})_12p_{3/2})_{5/2}$	QR	1478.4		1473.5	1477.8	4.61(-24)	2.40(-20)	8.59(-24)
	$(1s_{1/2}2p_{1/2}^22p_{3/2})_{3/2}$	QR	1478.6		1473.6	1477.9	3.03(-24)	1.55(-20)	5.75(-24)
	$((1s_{1/2}2p_{1/2})_12p_{3/2})_{3/2}$	QR	1481.4		1476.2	1480.5	1.34(-25)	4.95(-22)	4.94(-25)
	$((1s_{1/2}2p_{1/2})_12p_{3/2})_{1/2}$	QR	1481.9		1476.8	1481.1	7.00(-25)	4.74(-23)	8.46(-25)
	$(1s_{1/2}2p_{1/2}^22p_{3/2})_{1/2}$	QR	1493.0		1488.2	1492.5	7.96(-23)	1.08(-20)	1.30(-22)

values. The sizes of contributions from different charge states can be distinguished from the detailed theoretical calculation in the mixed spectrum. For instance, the first three peaks are mainly due to the KLL resonance contributions of He-like Si^{12+} ions, Li-like Si^{11+} and H-like Si^{13+} ions.

B. EIE rate coefficients

In the EIE process, both DE and RE processes need to be considered to explain the experimental rate coefficients in the energy range 1.8–2.5 keV. The mainly DE and RE processes for Si^{13+} , Si^{12+} , Si^{11+} , and Si^{10+} ions are described as Eqs. (20)–(23). Where Eqs. (20a)–(23a) are for DE processes, Eqs. (20b)–(23b) are for RE processes in which first a doubly excited state is formed by dielectronic capture (DC), followed by an autoionization process to the DE final states, leaving the

charge state of the ion unchanged. The excited states decay by x-ray emission, which are given by Eqs. (20c)–(23c).

In order to illustrate the reliability of the present calculations, some DE excitation energies from the ground states of Si^{13+} , Si^{12+} , Si^{11+} , and Si^{10+} ions are listed in Table III and compared with the NIST values [38]. It is found that the theoretical results agree reasonably well with the experimental results (within 0.12%). In Fig. 4, the contributions of the DE and RE excitation-rate coefficients for silicon ions are shown. As seen clearly from the four figures, the resonant contribution is quite large. Similar phenomena have also been reported, e.g., by Pindzola *et al.* [39] and Jiang *et al.* [40]. The graphs in Fig. 4 show that the contributions are different in different energy regions for each of the ion charges.

In Fig. 5, the synthesized EIE rate coefficients of silicon ions are compared with the EBIT experimental measurements [27]. In our theoretical simulation, the separate contributions

TABLE II. The resonance energies (in eV) and resonance strengths (in $\text{cm}^2 \text{ eV}$) for Si^{13+} , Si^{12+} , Si^{11+} , and Si^{10+} ions in the *KLM* manifold. Only the resonance states with $S_d > 10^{-22}$ ($\text{cm}^2 \text{ eV}$) are tabulated for the Si^{11+} and Si^{10+} ions. [$a(b)$ denotes $a \times 10^b$.]

Ions	Resonance states	Type	Resonance energies	Resonance strengths
Si^{13+}	$(2s_{1/2}3s_{1/2})_1$	DR	1733.4	1.15(-21)
	$(2s_{1/2}3p_{3/2})_1$	DR	1735.1	3.25(-22)
	$(2s_{1/2}3s_{1/2})_0$	DR	1737.4	4.86(-21)
	$(2p_{1/2}3s_{1/2})_0$	DR	1738.1	2.57(-21)
	$(2p_{1/2}3s_{1/2})_1$	DR	1738.5	7.91(-21)
	$(2p_{1/2}3p_{1/2})_1$	DR	1738.6	2.76(-24)
	$(2s_{1/2}3p_{3/2})_2$	DR	1739.3	1.25(-20)
	$(2p_{1/2}3p_{3/2})_2$	DR	1739.5	2.08(-21)
	$(2s_{1/2}3p_{1/2})_0$	DR	1740.0	9.95(-22)
	$(2s_{1/2}3p_{1/2})_1$	DR	1740.2	1.92(-21)
	$(2p_{3/2}3p_{3/2})_1$	DR	1740.2	8.43(-24)
	$(2p_{3/2}3p_{3/2})_3$	DR	1740.4	5.86(-23)
	$(2p_{3/2}3s_{1/2})_2$	DR	1740.6	3.36(-22)
	$(2p_{1/2}3d_{3/2})_2$	DR	1743.2	9.96(-21)
	$(2p_{1/2}3p_{1/2})_0$	DR	1744.1	3.38(-22)
	$(2p_{1/2}3d_{5/2})_3$	DR	1744.2	1.67(-20)
	$(2s_{1/2}3p_{3/2})_1$	DR	1744.6	6.27(-24)
	$(2p_{3/2}3d_{5/2})_2$	DR	1744.7	2.58(-21)
	$(2p_{1/2}3p_{3/2})_2$	DR	1744.9	5.21(-20)
	$(2p_{3/2}3d_{5/2})_4$	DR	1745.0	2.13(-20)
	$(2p_{3/2}3p_{3/2})_2$	DR	1745.7	5.14(-20)
	$(2s_{1/2}3d_{3/2})_1$	DR	1746.2	2.82(-21)
	$(2s_{1/2}3d_{5/2})_2$	DR	1746.4	8.67(-21)
	$(2s_{1/2}3d_{5/2})_3$	DR	1746.6	6.89(-21)
	$(2p_{3/2}3p_{3/2})_1$	DR	1747.3	1.81(-22)
	$(2p_{1/2}3d_{3/2})_1$	DR	1747.6	3.97(-21)
	$(2p_{3/2}3d_{3/2})_2$	DR	1748.1	2.13(-22)
	$(2p_{3/2}3d_{5/2})_3$	DR	1748.5	7.62(-22)
	$(2p_{3/2}3s_{1/2})_1$	DR	1748.9	2.68(-20)
	$(2p_{3/2}3d_{5/2})_2$	DR	1751.3	2.95(-23)
	$(2p_{3/2}3d_{3/2})_1$	DR	1751.5	6.20(-22)
	$(2p_{3/2}3d_{3/2})_0$	DR	1751.7	5.23(-24)
	$(2s_{1/2}3d_{5/2})_2$	DR	1752.4	2.79(-20)
	$(2p_{3/2}3d_{3/2})_3$	DR	1754.2	4.82(-20)
	$(2p_{3/2}3d_{5/2})_1$	DR	1755.9	3.41(-21)
	$(2p_{3/2}3p_{3/2})_0$	DR	1756.9	3.58(-21)
	$((1s_{1/2}2s_{1/2})_13s_{1/2})_{3/2}$	DR	1599.9	1.23(-27)
	$((1s_{1/2}2s_{1/2})_13s_{1/2})_{1/2}$	DR	1605.5	1.39(-21)
	$((1s_{1/2}2s_{1/2})_13p_{1/2})_{1/2}$	DR	1608.1	2.98(-24)
	$((1s_{1/2}2s_{1/2})_13p_{1/2})_{3/2}$	DR	1608.2	1.33(-22)
	$((1s_{1/2}2s_{1/2})_13p_{3/2})_{5/2}$	DR	1608.4	6.56(-25)
	$((1s_{1/2}2s_{1/2})_13p_{3/2})_{3/2}$	DR	1609.2	6.66(-21)
	$((1s_{1/2}2s_{1/2})_13p_{3/2})_{1/2}$	DR	1609.2	2.92(-21)
	$((1s_{1/2}2s_{1/2})_13d_{3/2})_{1/2}$	DR	1613.1	2.67(-25)
	$((1s_{1/2}2s_{1/2})_13d_{3/2})_{3/2}$	DR	1613.1	8.80(-25)
	$((1s_{1/2}2s_{1/2})_13d_{5/2})_{5/2}$	DR	1613.2	2.14(-25)
	$((1s_{1/2}2s_{1/2})_13d_{5/2})_{7/2}$	DR	1613.3	4.89(-27)
	$((1s_{1/2}2s_{1/2})_13d_{3/2})_{5/2}$	DR	1616.4	4.03(-21)
	$((1s_{1/2}2s_{1/2})_13d_{5/2})_{3/2}$	DR	1616.4	3.02(-21)
	$((1s_{1/2}2s_{1/2})_03s_{1/2})_{1/2}$	DR	1617.0	8.26(-21)
	$((1s_{1/2}2p_{1/2})_03s_{1/2})_{1/2}$	DR	1618.0	3.02(-25)
	$((1s_{1/2}2p_{1/2})_13s_{1/2})_{3/2}$	DR	1618.3	1.05(-22)
	$((1s_{1/2}2p_{3/2})_23s_{1/2})_{5/2}$	DR	1619.0	5.84(-25)
	$((1s_{1/2}2s_{1/2})_03p_{1/2})_{1/2}$	DR	1622.3	1.64(-22)
	$((1s_{1/2}2s_{1/2})_03p_{3/2})_{3/2}$	DR	1622.6	2.30(-23)
	$((1s_{1/2}2p_{1/2})_03p_{1/2})_{1/2}$	DR	1623.3	2.29(-24)
	$((1s_{1/2}2p_{1/2})_13p_{1/2})_{3/2}$	DR	1623.5	4.17(-23)
	$((1s_{1/2}2p_{1/2})_13p_{3/2})_{5/2}$	DR	1624.0	3.01(-22)

TABLE II. (*Continued.*)

Ions	Resonance states	Type	Resonance energies	Resonance strengths
Si^{12+}	$((1s_{1/2}2p_{3/2})_23p_{3/2})_{7/2}$	DR	1624.6	3.01(-27)
	$((1s_{1/2}2p_{1/2})_13p_{3/2})_{1/2}$	DR	1624.7	2.97(-23)
	$((1s_{1/2}2p_{3/2})_23p_{3/2})_{3/2}$	DR	1624.8	2.71(-22)
	$((1s_{1/2}2p_{1/2})_13s_{1/2})_{1/2}$	DR	1625.8	1.34(-20)
	$((1s_{1/2}2p_{1/2})_13p_{3/2})_{3/2}$	DR	1626.5	4.47(-23)
	$((1s_{1/2}2p_{1/2})_13p_{1/2})_{1/2}$	DR	1626.6	5.17(-24)
	$((1s_{1/2}2p_{3/2})_23s_{1/2})_{3/2}$	DR	1626.7	1.76(-20)
	$((1s_{1/2}2p_{3/2})_23p_{1/2})_{3/2}$	DR	1627.1	1.79(-23)
	$((1s_{1/2}2p_{3/2})_23p_{3/2})_{5/2}$	DR	1627.3	3.66(-22)
	$((1s_{1/2}2p_{1/2})_03d_{3/2})_{3/2}$	DR	1627.5	4.45(-25)
	$((1s_{1/2}2p_{1/2})_13d_{3/2})_{5/2}$	DR	1627.8	1.54(-22)
	$((1s_{1/2}2p_{1/2})_13d_{5/2})_{7/2}$	DR	1628.2	1.46(-22)
	$((1s_{1/2}2p_{3/2})_23d_{5/2})_{9/2}$	DR	1628.6	2.64(-29)
	$((1s_{1/2}2p_{1/2})_13d_{5/2})_{3/2}$	DR	1628.9	1.15(-22)
	$((1s_{1/2}2p_{3/2})_23p_{5/2})_{5/2}$	DR	1629.0	2.35(-23)
	$((1s_{1/2}2s_{1/2})_03d_{3/2})_{3/2}$	DR	1629.4	7.48(-21)
	$((1s_{1/2}2s_{1/2})_03d_{5/2})_{5/2}$	DR	1629.6	5.46(-21)
	$((1s_{1/2}2p_{1/2})_13p_{3/2})_{3/2}$	DR	1630.0	3.05(-20)
	$((1s_{1/2}2p_{3/2})_23p_{3/2})_{5/2}$	DR	1630.7	6.34(-20)
	$((1s_{1/2}2p_{1/2})_13d_{3/2})_{1/2}$	DR	1631.2	9.41(-23)
	$((1s_{1/2}2p_{3/2})_23d_{3/2})_{3/2}$	DR	1631.3	7.89(-23)
	$((1s_{1/2}2p_{3/2})_23d_{3/2})_{5/2}$	DR	1631.5	2.62(-23)
	$((1s_{1/2}2p_{3/2})_23d_{5/2})_{7/2}$	DR	1631.7	9.35(-23)
	$((1s_{1/2}2p_{3/2})_13s_{1/2})_{3/2}$	DR	1631.8	3.11(-20)
	$((1s_{1/2}2p_{3/2})_13s_{1/2})_{1/2}$	DR	1631.9	1.97(-20)
	$((1s_{1/2}2p_{1/2})_13d_{5/2})_{5/2}$	DR	1632.6	6.70(-22)
	$((1s_{1/2}2p_{3/2})_23d_{5/2})_{5/2}$	DR	1633.0	1.32(-23)
	$((1s_{1/2}2p_{3/2})_23d_{3/2})_{3/2}$	DR	1633.3	7.45(-23)
	$((1s_{1/2}2p_{3/2})_23d_{3/2})_{1/2}$	DR	1633.4	2.30(-23)
	$((1s_{1/2}2p_{3/2})_23d_{3/2})_{7/2}$	DR	1633.5	4.55(-22)
	$((1s_{1/2}2p_{3/2})_23p_{3/2})_{1/2}$	DR	1634.2	8.09(-21)
	$((1s_{1/2}2p_{3/2})_23d_{5/2})_{3/2}$	DR	1636.3	7.40(-22)
	$((1s_{1/2}2p_{3/2})_23d_{5/2})_{1/2}$	DR	1636.8	3.47(-22)
	$((1s_{1/2}2p_{3/2})_13p_{1/2})_{3/2}$	DR	1638.1	9.71(-20)
	$((1s_{1/2}2p_{3/2})_13p_{3/2})_{5/2}$	DR	1638.1	1.45(-19)
	$((1s_{1/2}2p_{3/2})_13p_{1/2})_{1/2}$	DR	1638.2	7.87(-24)
	$((1s_{1/2}2p_{3/2})_13p_{3/2})_{3/2}$	DR	1638.6	1.76(-20)
	$((1s_{1/2}2p_{3/2})_13d_{3/2})_{3/2}$	DR	1641.9	1.25(-26)
	$((1s_{1/2}2p_{3/2})_13d_{5/2})_{5/2}$	DR	1642.0	1.21(-21)
	$((1s_{1/2}2p_{3/2})_13p_{3/2})_{1/2}$	DR	1642.2	2.18(-20)
	$((1s_{1/2}2p_{3/2})_13d_{5/2})_{7/2}$	DR	1642.9	1.01(-19)
	$((1s_{1/2}2p_{3/2})_13d_{3/2})_{5/2}$	DR	1643.2	7.42(-20)
	$((1s_{1/2}2p_{3/2})_13d_{3/2})_{1/2}$	DR	1645.7	1.51(-22)
	$((1s_{1/2}2p_{3/2})_13d_{5/2})_{3/2}$	DR	1645.9	3.66(-22)
	$(1s_{1/2}2s_{1/2}^2)_13s_{1/2})_1$	DR	1610.5	7.15(-22)
	$(1s_{1/2}2s_{1/2}^2)_13s_{1/2})_0$	DR	1613.7	1.47(-22)
	$((1s_{1/2}2s_{1/2})_12p_{1/2})_{1/2}3s_{1/2})_0$	DR	1624.4	1.77(-22)
	$((1s_{1/2}2s_{1/2})_12p_{1/2})_{3/2}3s_{1/2})_1$	DR	1624.6	5.04(-22)
	$((1s_{1/2}2s_{1/2})_12p_{3/2})_{5/2}3s_{1/2})_2$	DR	1625.2	6.80(-22)
	$((1s_{1/2}2s_{1/2})_12p_{3/2})_{5/2}3p_{3/2})_1$	DR	1626.1	1.04(-22)
	$((1s_{1/2}2s_{1/2})_12p_{3/2})_{5/2}3p_{3/2})_2$	DR	1626.3	3.58(-22)
	$(1s_{1/2}2s_{1/2}^2)_13d_{5/2})_2$	DR	1629.0	1.55(-22)
	$((1s_{1/2}2s_{1/2})_12p_{1/2})_{1/2}3p_{3/2})_1$	DR	1630.9	9.34(-21)
	$((1s_{1/2}2s_{1/2})_12p_{1/2})_{3/2}3p_{3/2})_2$	DR	1631.1	1.55(-20)
	$((1s_{1/2}2s_{1/2})_12p_{3/2})_{5/2}3p_{1/2})_3$	DR	1631.5	2.15(-20)
	$((1s_{1/2}2s_{1/2})_12p_{3/2})_{5/2}3p_{3/2})_1$	DR	1634.5	5.91(-21)
	$((1s_{1/2}2s_{1/2})_12p_{3/2})_{5/2}3d_{3/2})_1$	DR	1636.8	1.80(-22)
	$((1s_{1/2}2s_{1/2})_12p_{3/2})_{5/2}3d_{3/2})_1$	DR	1636.8	1.12(-22)

TABLE II. (*Continued.*)

Ions	Resonance states	Type	Resonance energies	Resonance strengths
Si^{10+}	$((1s_{1/2}2p_{3/2}^2)_{1/2}3p_{1/2})_1$	TR	1685.4	7.58(-22)
	$((1s_{1/2}2p_{3/2}^2)_{1/2}3p_{3/2})_2$	TR	1685.5	1.26(-21)
	$((1s_{1/2}2p_{3/2}^2)_{1/2}3p_{3/2})_1$	TR	1687.7	1.57(-22)
	$((1s_{1/2}2p_{3/2}^2)_{1/2}3d_{5/2})_3$	TR	1692.7	3.06(-22)
	$((1s_{1/2}2p_{3/2}^2)_{1/2}3d_{5/2})_2$	TR	1692.8	2.13(-22)
	$((1s_{1/2}2p_{3/2}^2)_{1/2}3d_{3/2})_1$	TR	1692.8	1.31(-22)
	$((1s_{1/2}2s_{1/2}^22p_{3/2})_23s_{1/2})_{3/2}$	DR	1639.3	1.98(-22)
	$((1s_{1/2}2s_{1/2}^22p_{3/2})_13s_{1/2})_{1/2}$	DR	1646.6	1.09(-22)
	$((1s_{1/2}2s_{1/2}^22p_{1/2})_13p_{3/2})_{3/2}$	DR	1649.5	5.51(-21)
	$((1s_{1/2}2s_{1/2}^22p_{3/2})_23p_{1/2})_{5/2}$	DR	1650.2	7.97(-21)
	$((1s_{1/2}2s_{1/2}^22p_{3/2})_23p_{3/2})_{1/2}$	DR	1652.4	1.06(-21)
	$((1s_{1/2}2s_{1/2}^22p_{3/2})_13p_{1/2})_{3/2}$	DR	1656.5	2.01(-20)
	$((1s_{1/2}2s_{1/2}^22p_{3/2})_13p_{3/2})_{5/2}$	DR	1656.6	3.33(-20)
	$((1s_{1/2}2s_{1/2}^22p_{3/2})_13p_{3/2})_{3/2}$	DR	1656.8	7.10(-21)
	$((1s_{1/2}2s_{1/2}^22p_{3/2})_13p_{3/2})_{1/2}$	DR	1659.5	6.22(-21)
	$((1s_{1/2}2s_{1/2}^22p_{3/2})_13d_{5/2})_{7/2}$	DR	1668.2	1.25(-20)
	$((1s_{1/2}2s_{1/2}^22p_{3/2})_13d_{3/2})_{5/2}$	DR	1668.5	9.04(-21)
	$((1s_{1/2}2s_{1/2}12p_{1/2})_{3/2}2p_{3/2})_33s_{1/2})_{5/2}$	TR	1668.5	3.85(-22)
	$((1s_{1/2}2s_{1/2}12p_{1/2})_{3/2}2p_{3/2})_23s_{1/2})_{3/2}$	TR	1668.5	3.17(-22)
	$((1s_{1/2}2s_{1/2}12p_{3/2})_12p_{3/2})_{3/2}$	TR	1669.2	1.94(-22)
	$((1s_{1/2}2s_{1/2}12p_{3/2})_13d_{3/2})_{1/2}$	DR	1669.7	2.42(-22)
	$((1s_{1/2}2s_{1/2}12p_{3/2})_13d_{5/2})_{3/2}$	DR	1669.8	4.64(-22)
	$((1s_{1/2}2s_{1/2}12p_{3/2})_13s_{1/2})_{1/2}$	TR	1679.1	3.10(-22)
	$((1s_{1/2}2s_{1/2}12p_{3/2})_13p_{1/2})_{3/2}$	TR	1687.1	1.53(-22)
	$((1s_{1/2}2s_{1/2}12p_{3/2})_13p_{3/2})_{1/2}$	TR	1687.3	1.24(-22)
	$((1s_{1/2}2s_{1/2}02p_{3/2})_03p_{3/2})_{3/2}$	TR	1700.3	2.20(-22)
	$((1s_{1/2}2s_{1/2}02p_{3/2})_03p_{1/2})_{1/2}$	TR	1700.3	1.10(-22)
	$((1s_{1/2}2s_{1/2}12p_{1/2})_{3/2}2p_{3/2})_13d_{3/2})_{3/2}$	TR	1709.0	1.15(-22)
	$((1s_{1/2}2s_{1/2}12p_{1/2})_{3/2}2p_{3/2})_13d_{5/2})_{5/2}$	TR	1709.0	1.92(-22)

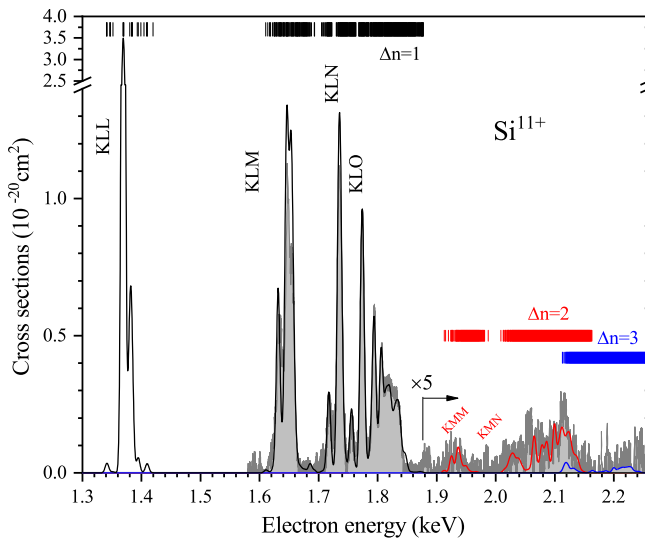


FIG. 2. Dielectronic recombination cross sections of Si^{11+} ($1s^22s\ ^2S_{1/2}$) in the ground state resulting from $\Delta n = 1$ (black line), $\Delta n = 2$ (red line), and $\Delta n = 3$ (blue line) resonances. The theoretical cross section was folded with the resolution function of a linewidth of 7 eV FWHM and is here compared to the experimental measurements by Kenntner *et al.* [17] (gray area). The colored vertical bars show the resonant positions for individual resonances.

from the different charge states (50% H-like Si^{13+} , 42% He-like Si^{12+} , 6% Li-like Si^{11+} , and 2% Be-like Si^{10+} target

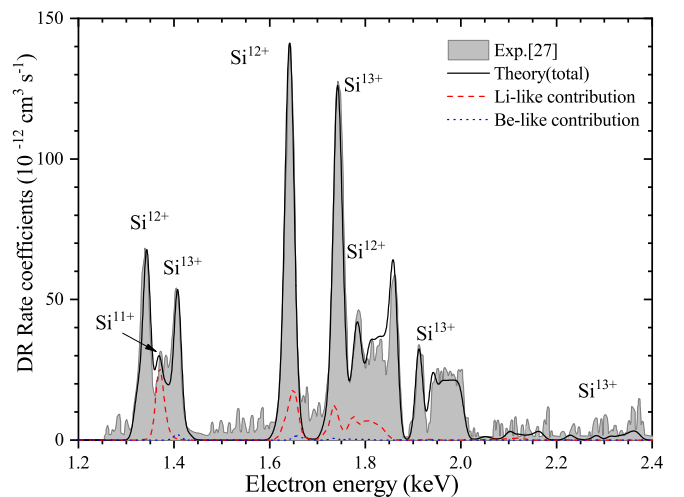


FIG. 3. The theoretical DR rate coefficients (black solid line) compared to the EBIT experimental results by Lindroth *et al.* [27] (gray area). The stronger peaks have been identified to come from H-like Si^{13+} (41%), He-like Si^{12+} (38%) ions, the red line and blue dotted line show the contributions from Li-like Si^{11+} (17%) and Be-like Si^{10+} (3%) ions, respectively.

TABLE III. The calculated DE excitation energies (units of eV) from the ground states to part of K -shell excited states of Si^{13+} , Si^{12+} , Si^{11+} , and Si^{10+} ions, compared with the NIST values [38]

Ions	Excited states	Excitation energy	
		This	NIST [38]
Si^{13+}	$1s_{1/2}$	0.0	0.0
	$2p_{1/2}$	2004.4	2004.3
	$2s_{1/2}$	2004.4	2004.4
	$2p_{3/2}$	2006.1	2006.1
	$3p_{1/2}$	2376.1	2376.1
	$3s_{1/2}$	2376.2	2376.1
	$3d_{3/2}$	2376.7	2376.6
	$3p_{3/2}$	2376.7	2376.6
	$3d_{5/2}$	2376.8	2376.8
	$1s^2 \ ^1S_0$	0.0	0.0
	$(1s_{1/2}2s_{1/2})_1$	1839.8	1839.4
	$(1s_{1/2}2p_{1/2})_0$	1855.1	1853.5
	$(1s_{1/2}2p_{1/2})_1$	1855.3	1853.8
	$(1s_{1/2}2s_{1/2})_0$	1855.8	1854.7
Si^{12+}	$(1s_{1/2}2p_{3/2})_2$	1856.2	1854.6
	$(1s_{1/2}2p_{3/2})_1$	1867.2	1865.0
	$(1s_{1/2}3s_{1/2})_1$	2174.7	2175.5
	$(1s_{1/2}3p_{1/2})_0$	2178.7	2179.4
	$(1s_{1/2}3p_{1/2})_1$	2178.8	2179.5
	$(1s_{1/2}3s_{1/2})_0$	2178.9	2179.5
	$(1s_{1/2}3p_{3/2})_2$	2179.0	2179.7
	$(1s_{1/2}3d_{3/2})_1$	2181.4	2181.9
	$(1s_{1/2}3d_{3/2})_2$	2181.4	2181.9
	$(1s_{1/2}3d_{5/2})_3$	2181.5	2182.0
	$(1s_{1/2}3d_{5/2})_2$	2181.7	2182.1
	$(1s_{1/2}3p_{3/2})_1$	2182.0	2182.6
	$1s^2 2s_{1/2}$	0.0	0.0
	$(1s_{1/2}2s_{1/2}^2)_{1/2}$	1820.9	1820.4
Si^{11+}	$((1s_{1/2}2s_{1/2})_12p_{1/2})_{1/2}$	1827.9	1826.6
	$((1s_{1/2}2s_{1/2})_12p_{1/2})_{3/2}$	1828.2	1826.8
	$((1s_{1/2}2s_{1/2})_12p_{3/2})_{5/2}$	1828.8	1827.5
	$((1s_{1/2}2s_{1/2})_02p_{1/2})_{1/2}$	1847.0	1845.0
	$((1s_{1/2}2s_{1/2})_02p_{3/2})_{3/2}$	1847.6	1845.5
	$(1s_{1/2}2p_{1/2}^2)_{1/2}$	1855.1	1851.9
	$((1s_{1/2}2p_{1/2})_02p_{3/2})_{3/2}$	1855.5	1852.4
	$(1s_{1/2}2p_{3/2}^2)_{5/2}$	1856.0	1852.9
	$((1s_{1/2}2s_{1/2})_12p_{3/2})_{1/2}$	1856.2	1854.0
	$((1s_{1/2}2s_{1/2})_02p_{3/2})_{3/2}$	1856.4	1853.8
	$((1s_{1/2}2p_{1/2})_12p_{3/2})_{5/2}$	1867.7	1863.8
	$((1s_{1/2}2p_{1/2})_02p_{3/2})_{3/2}$	1867.8	1864.0
	$((1s_{1/2}2p_{1/2})_12p_{3/2})_{1/2}$	1871.2	1866.9
	$(1s_{1/2}2p_{3/2}^2)_{3/2}$	1872.1	1867.8
	$(1s_{1/2}2p_{3/2}^2)_{1/2}$	1885.0	1880.5

TABLE III. (*Continued.*)

Ions	Excited states	Excitation energy	
		This	NIST [38]
Si^{10+}	$((1s_{1/2}2s_{1/2})_13d_{5/2})_{3/2}$	2144.3	
	$((1s_{1/2}2s_{1/2})_03s_{1/2})_{1/2}$	2145.4	
	$((1s_{1/2}2s_{1/2})_03p_{1/2})_{1/2}$	2151.9	
	$((1s_{1/2}2s_{1/2})_03p_{3/2})_{3/2}$	2152.3	
	$((1s_{1/2}2s_{1/2})_03d_{3/2})_{3/2}$	2157.3	
	$((1s_{1/2}2s_{1/2})_03d_{5/2})_{5/2}$	2157.4	
	$1s^22s^2{}^1S_0$	0.0	0.0
	$(1s_{1/2}2s_{1/2}^22p_{1/2})_0$	1819.2	
	$(1s_{1/2}2s_{1/2}^22p_{1/2})_1$	1819.4	
	$(1s_{1/2}2s_{1/2}^22p_{3/2})_2$	1820.1	
	$((1s_{1/2}2s_{1/2})_12p_{1/2}^2)_1$	1825.5	
	$((1s_{1/2}2s_{1/2})_12p_{1/2})_{1/2}2p_{3/2})_2$	1825.8	
	$((1s_{1/2}2s_{1/2})_12p_{3/2}^2)_3$	1826.2	
	$(1s_{1/2}2s_{1/2}^22p_{3/2})_1$	1830.3	1828.6
	$((1s_{1/2}2s_{1/2})_12p_{1/2})_{3/2}2p_{3/2})_3$	1848.1	1844.5
	$((1s_{1/2}2s_{1/2})_12p_{1/2})_{3/2}2p_{3/2})_2$	1848.2	1844.6
	$((1s_{1/2}2s_{1/2})_12p_{1/2})_{1/2}2p_{3/2})_1$	1848.2	1844.7
	$((1s_{1/2}2s_{1/2})_12p_{1/2})_{3/2}2p_{3/2})_0$	1848.3	1844.8
	$((1s_{1/2}2s_{1/2})_02p_{1/2})_{1/2}2p_{3/2})_1$	1848.7	1845.2
	$((1s_{1/2}2s_{1/2})_12p_{3/2}^2)_2$	1849.3	1845.8
	$((1s_{1/2}2s_{1/2})_12p_{3/2}^2)_1$	1859.0	
	$((1s_{1/2}2s_{1/2})_02p_{1/2})_{1/2}2p_{3/2})_2$	1862.3	1858.6
	$((1s_{1/2}2s_{1/2})_12p_{1/2})_{3/2}2p_{3/2})_0$	1863.2	
	$((1s_{1/2}2p_{1/2})_12p_{3/2}^2)_2$	1863.4	1859.7
	$((1s_{1/2}2s_{1/2})_02p_{1/2})_{1/2}2p_{3/2})_1$	1863.5	
	$((1s_{1/2}2s_{1/2})_02p_{3/2}^2)_2$	1867.0	
	$((1s_{1/2}2s_{1/2})_12p_{1/2})_{3/2}2p_{3/2})_1$	1872.5	1867.4
	$((1s_{1/2}2s_{1/2})_02p_{3/2}^2)_0$	1873.3	
	$((1s_{1/2}2p_{1/2})_12p_{3/2}^2)_3$	1878.0	
	$((1s_{1/2}2p_{1/2})_02p_{3/2}^2)_2$	1878.2	
	$((1s_{1/2}2p_{1/2})_12p_{3/2}^2)_1$	1878.3	
	$((1s_{1/2}2p_{1/2})_12p_{3/2}^2)_1$	1883.6	
	$((1s_{1/2}2p_{1/2})_12p_{3/2}^2)_2$	1888.0	1881.6
	$((1s_{1/2}2p_{1/2})_12p_{3/2}^2)_1$	1888.8	
	$((1s_{1/2}2p_{1/2})_02p_{3/2}^2)_0$	1888.8	
	$(1s_{1/2}2p_{3/2}^2)_2$	1889.1	1883.2
	$(1s_{1/2}2p_{3/2}^2)_1$	1898.9	1892.2
	$(1s_{1/2}2s_{1/2}^23s_{1/2})_1$	2094.0	
	$(1s_{1/2}2s_{1/2}^23s_{1/2})_0$	2097.7	
	$(1s_{1/2}2s_{1/2}^23p_{1/2})_0$	2100.3	
	$(1s_{1/2}2s_{1/2}^23p_{1/2})_1$	2100.4	
	$(1s_{1/2}2s_{1/2}^23p_{3/2})_2$	2100.7	
	$(1s_{1/2}2s_{1/2}^23p_{1/2})_1$	2105.8	
	$(1s_{1/2}2s_{1/2}^23d_{3/2})_1$	2113.2	
	$(1s_{1/2}2s_{1/2}^23d_{3/2})_2$	2113.2	
	$(1s_{1/2}2s_{1/2}^23d_{5/2})_3$	2113.3	
	$(1s_{1/2}2s_{1/2}^23d_{3/2})_2$	2113.5	

ions) are considered. As can be seen there, the theoretical rate coefficients are in overall excellent agreement with the experimental results of Ref. [27]. Of course, there are still certain differences between theoretical and experimental resonance peaks in certain energy ranges. For instance, there is a slight difference around the electron energy 1.85 keV. Probably some RE contributions are missing from the calcu-

lation. In order to find a possible explanation, we calculated the RE rate coefficients of metastable states and other excited states, but did not find any obvious excitations in this energy region. Another possible reason could be that there are contributions to the rate coefficient from other silicon charge states aside from those considered. In addition, the theoretical values are slightly lower than the experimental values in the

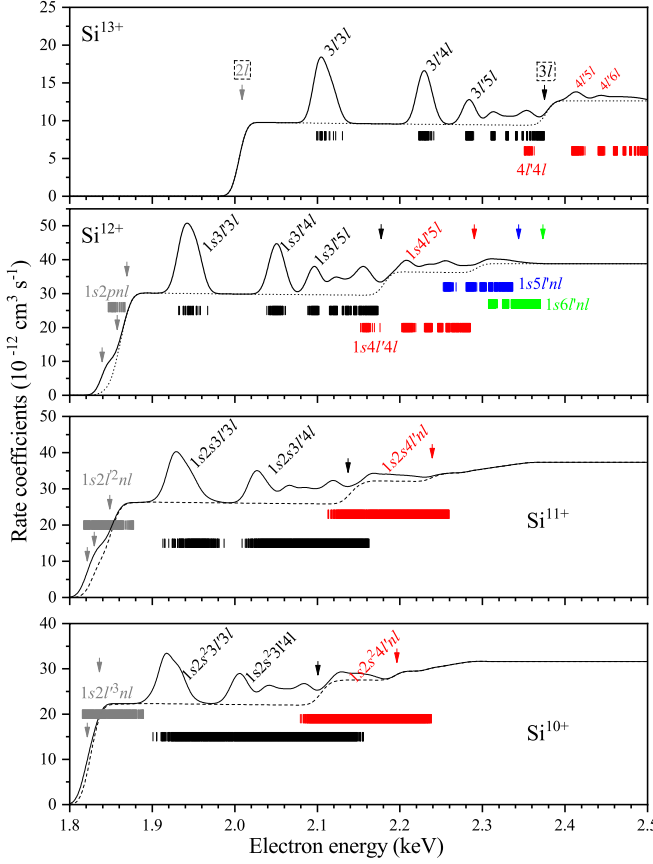


FIG. 4. The theoretical EIE rate coefficients of Si^{13+} , Si^{12+} , Si^{11+} , and Si^{10+} ions as functions of electron energy. The black solid lines describe the total (RE+DE) rate coefficients and dotted line for the DE. The vertical arrows show $1s \rightarrow n'l'$ excitation thresholds. Colored vertical bars show resonance positions. The dominant resonance peaks belonging to different resonance groups are labeled.

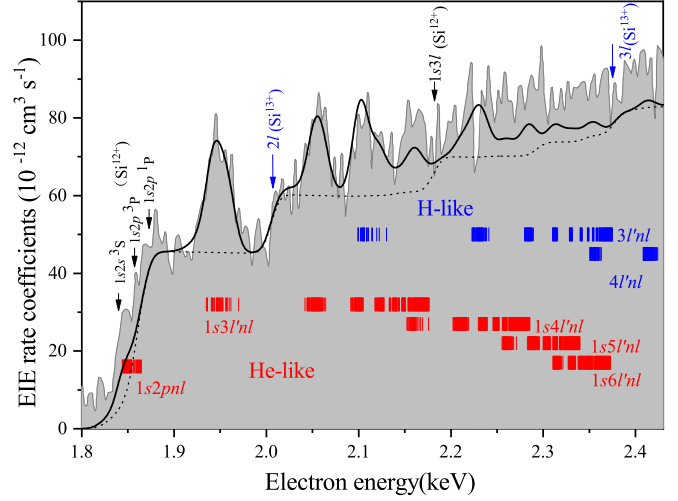


FIG. 5. Synthesized EIE rate coefficients (black solid line) of Si^{13+} , Si^{12+} , Si^{11+} , and Si^{10+} ions as formulated by Eqs. (20)–(23), compared with the EBIT experimental results by Lindroth *et al.* [27] (gray area). The DE rate coefficients are given by the dotted line. The vertical arrows show $1s \rightarrow n'l'$ excitation thresholds of H-like and He-like silicon ions, and the colored vertical bars show dominant RE resonance positions.

electron energy range between 2.15 and 2.4 keV. We think that this could be due to collisional cascade processes and high n' [see Eqs. (20)–(23)] resonance excitations [41], that have not been taken into account in the calculations. It should be noted that in the experiment, the EIE rate coefficient is not directly measured separately from the DR rate coefficients. Instead, they measured the total photo rate-coefficient spectrum and the DR rate-coefficient spectrum separately, and then the EIE rate-coefficient spectrum is extracted based on these two spectra:

$$\varepsilon e^- + \text{Si}^{13+}(1s) \rightarrow \begin{cases} \varepsilon' e^- + [\text{Si}^{13+}(n'l')]^* & (n' = 2-3, \text{ DE}), \\ \varepsilon' e^- + [\text{Si}^{12+}(n'l'n'l)]^{**} \rightarrow [\text{Si}^{13+}(n'l')]^* & (n' = 3-4, n = 3-30, \text{ RE}) \end{cases} \quad (20a)$$

$$(20b)$$

$$\rightarrow \text{Si}^{13+}(1s) + h\nu, \quad (20c)$$

$$\varepsilon e^- + \text{Si}^{12+}(1s^2) \rightarrow \begin{cases} \varepsilon' e^- + [\text{Si}^{12+}(1sn'l')]^* & (n' = 2-10, \text{ DE}), \\ \varepsilon' e^- + [\text{Si}^{11+}(1sn'l'n'l)]^{**} \rightarrow [\text{Si}^{12+}(1sn'l')]^* & (n' = 2-7, n = 2-30, \text{ RE}) \end{cases} \quad (21a)$$

$$(21b)$$

$$\rightarrow \text{Si}^{12+}(1s^2) + h\nu, \quad (21c)$$

$$\varepsilon e^- + \text{Si}^{11+}(1s^22s) \rightarrow \begin{cases} \varepsilon' e^- + [\text{Si}^{11+}(1s2ln'l')]^* & (n' = 2-10, \text{ DE}), \\ \varepsilon' e^- + [\text{Si}^{10+}(1s2sn'l'n'l)]^{**} \rightarrow [\text{Si}^{11+}(1s2ln'l')]^* & (n' = 2-4, n = 2-30, \text{ RE}) \end{cases} \quad (22a)$$

$$(22b)$$

$$\rightarrow \text{Si}^{11+}(1s^22s) + h\nu, \quad (22c)$$

$$\varepsilon e^- + \text{Si}^{10+}(1s^22s^2) \rightarrow \begin{cases} \varepsilon' e^- + [\text{Si}^{10+}(1s2l^2n'l')]^* & (n' = 2-10, \text{ DE}), \\ \varepsilon' e^- + [\text{Si}^{9+}(1s2l^2n'l'n'l)]^{**} \rightarrow [\text{Si}^{10+}(1s2l^2n'l')]^* & (n' = 2-4, n = 2-30, \text{ RE}) \end{cases} \quad (23a)$$

$$(23b)$$

$$\rightarrow \text{Si}^{10+}(1s^22s^2) + h\nu. \quad (23c)$$

IV. CONCLUSIONS

We demonstrate in this paper that the FAC code based on a fully relativistic distorted-wave approach is able to calculate photorecombination rate coefficients of few-electron $\text{Si}^{13+} \sim \text{Si}^{10+}$ ions to a high accuracy of a few percent in the rate scale and better than 0.1% in the energy scale. This is concluded from comparisons with recent experimental results. Our theoretical DR rate coefficients are in very good agreement with the experimental results of Ref. [27] for H-like Si^{13+} and He-like Si^{12+} ions. For Li-like Si^{11+} ions, there is in part a disagreement found with the experiment [27], but here our calculation agrees somewhat better with the data from Ref. [17]. Also, the DR rate coefficients for $\Delta n = 2$ and 3 transitions of Si^{13+} , Si^{12+} , Si^{11+} , and Si^{10+} ions were calculated and found in good agreement with the experiments, although they are much smaller than the $\Delta n = 1$ rate coefficients. We calculate the direct and resonance EIE rate coefficients of Si^{13+} , Si^{12+} , Si^{11+} , and Si^{10+} ions and found the total EIE rate coefficients in excellent agreement with the experimental results [27]. It should be noted that in a certain energy range, DR and EIE processes coexist. A large interest concerns, therefore,

a comparison of the photorecombination rate coefficients in absolute scale, as these are of particular interest for plasma applications. Based on the detailed calculation of DR and EIE rate coefficients, we combined both rate coefficients and found good agreement within the statistical and systematic error bars of the experiment.

ACKNOWLEDGMENTS

The work was supported by the National Key Research and Development Program of China under Grants No. 2017YFA0402300, the Natural Science Foundation of China (Grants No. 12064041, No. U1530142, No. 11564036, No. 11774292, No. 11464042, and No. 11874051), the Funds for innovative Fundamental Research Group Project of Gansu Province (Grant No. 20JR5RA541), and the Natural Sciences Foundation of the Gansu Province for Young Scholars (Grant No. 18JR3RA100). R.S. acknowledges the hospitality of the Key Laboratory of Atomic and Molecular Physics during his visits.

-
- [1] Y. Hahn, Electron-ion recombination processes—an overview, *Rep. Prog. Phys.* **60**, 691 (1997).
 - [2] A. Burgess, Dielectronic recombination and the temperature of the solar corona, *Astrophys. J.* **139**, 776 (1964).
 - [3] D. A. Gurnett and A. Bhattacharjee, *Introduction to Plasma Physics: With Space and Laboratory Applications* (Cambridge University Press, Cambridge, 2005).
 - [4] C. W. Danforth and J. M. Shull, The low-z intergalactic medium. III. H and Metal Absorbers at $z < 0.4$, *Astrophys. J.* **679**, 194 (2008).
 - [5] R. Pugno, A. Kallenbach, D. Bolshukhin, R. Dux, J. Gafert, R. Neu, V. Rohde, K. Schmidtmann, W. Ullrich, and U. Wenzel, ASDEX Upgrad Team, Spectroscopic investigation on the impurity influxes of carbon and silicon in the ASDEX upgrade experiment, *J. Nucl. Mater.* **290**, 308 (2001).
 - [6] E. Anders and N. Grevesse, Abundances of the elements: Meteoritic and solar, *Geochim. Cosmochim. Acta* **53**, 197 (1989).
 - [7] M. Güdel and Y. Nazé, X-ray spectroscopy of stars, *Astron. Astrophys. Rev.* **17**, 309 (2009).
 - [8] H. Lehmann, A. Tkachenko, L. Fraga, V. Tsymbal, and D. E. Mkrtchian, The helium weak silicon star HR 7224 II. Doppler Imaging analysis, *Astron. Astrophys.* **471**, 941 (2007).
 - [9] A. Decourchelle, J. L. Sauvageot, M. Audard, B. Aschenbach, S. Sembay, R. Rothenflug, J. Ballet, T. Stadlbauer, and R. G. West, XMM-Newton observation of the Tycho supernova remnant, *Astron. Astrophys.* **365**, L218 (2001).
 - [10] J. D. T. Smith, L. Rudnick, T. Delaney, J. Rho, H. Gomez, T. Kozasa, W. Reach, and K. Isensee, Spitzer spectral mapping of supernova remnant cassiopeia A, *Astrophys. J.* **693**, 713 (2009).
 - [11] M. Sako, S. M. Kahn, F. Paerels, and D. A. Liedahl, The Chandra high-energy transmission grating observation of an X-ray ionization cone in markarian 3, *Astrophys. J.* **543**, L115 (2000).
 - [12] R. A. Simcoe, P. W. Sullivan, K. L. Cooksey, M. M. Kao, M. S. Matejek, and A. J. Burgasser, Extremely metal-poor gas at a redshift of 7, *Nature (London)* **492**, 79 (2012).
 - [13] O. Vilhu, P. Hakala, D. C. Hannikainen, M. McCollough, and K. Koljonen, Orbital modulation of X-ray emission lines in Cygnus X-3, *Astron. Astrophys.* **501**, 679 (2009).
 - [14] R. Schuch, in *Cooler Storage Rings: New Tools for Atomic Physics in Review of Fundamental Processes and Applications of Atoms and Ions*, edited by C. D. Lin (World Scientific, Singapore, 1993), p. 169.
 - [15] R. E. Marrs, M. A. Levine, D. A. Knapp, and J. R. Henderson, Measurement of Electron-Impact–Excitation Cross Sections for Very Highly Charged ions, *Phys. Rev. Lett.* **60**, 1715 (1988).
 - [16] G. Kilgus, J. Berger, P. Blatt, M. Grieser, D. Habs, B. Hochadel, E. Jaeschke, D. Krämer, R. Neumann, G. Neureither, W. Ott, D. Schwalm, M. Steck, R. Stokstad, E. Szumlak, A. Wolf, R. Schuch, A. Müller, and M. Wagner, Dielectronic Recombination of Hydrogenlike Oxygen in A Heavy-ion Storage Ring, *Phys. Rev. Lett.* **64**, 737 (1990).
 - [17] J. Kenntner, J. Linkemann, N. R. Badnell, C. Broude, D. Habs, G. Hofmann, A. Müller, M. S. Pindzola, E. Salzborn, D. Schwalm, and A. Wolf, Resonant electron impact ionization and recombination of Li-like Cl^{14+} and Si^{11+} at the Heidelberg Test Storage Ring, *Nucl. Instrum. Methods Phys. Res., Sect. B* **98**, 142 (1995).
 - [18] I. Orban, P. Glans, Z. Altun, E. Lindroth, A. Källberg, and R. Schuch, Determination of the recombination rate coefficients for Na-like SiIV forming Mg-like SiIII, *Astron. Astrophys.* **459**, 291 (2006).
 - [19] I. Orban, E. Lindroth, P. Glans, and R. Schuch, Spectroscopic study of doubly excited states in Mg-like Si using dielectronic recombination, *J. Phys. B: At., Mol. Opt. Phys.* **40**, 1063 (2007).
 - [20] I. Orban, S. D. Loch, S. Böhm, and R. Schuch, Recombination rate coefficients of Be-like Si, *Astrophys. J.* **721**, 1603 (2010).

- [21] T. M. Baumann, Z. Harman, J. Stark, C. Beilmann, G. Liang, P. H. Mokler, J. Ullrich, and J. R. Crespo López-Urrutia, Contributions of dielectronic, trielectronic, and metastable channels to the resonant intershell recombination of highly charged silicon ions, *Phys. Rev. A* **90**, 052704 (2014).
- [22] D. Bernhardt, A. Becker, C. Brandau, M. Grieser, M. Hahn, C. Krantz, M. Lestinsky, O. Novotný, R. Repnow, D. W. Savin, K. Spruck, A. Wolf, A. Müller, and S. Schippers, Absolute rate coefficients for photorecombination of beryllium-like and boron-like silicon ions, *J. Phys. B: At., Mol. Opt. Phys.* **49**, 074004 (2016).
- [23] S. Chantrenne, P. Beiersdorfer, R. Cauble, and M. B. Schneider, Measurement of Electron Impact Excitation Cross Sections for Heliumlike Titanium, *Phys. Rev. Lett.* **69**, 265 (1992).
- [24] S. Mahmood, S. Ali, I. Orban, S. Tashenov, E. Lindroth, and R. Schuch, Recombination and electron impact excitation rate coefficients for S XV and S XVI, *Astrophys. J.* **754**, 86 (2012).
- [25] N. Hell, G. V. Brown, J. Wilms, V. Grinberg, J. Clementson, D. Liedahl, F. S. Porter, R. L. Kelley, C. A. Kilbourne, and P. Beiersdorfer, Laboratory measurements of the K-shell transition energies in L-shell ions of Si and S, *Astrophys. J.* **830**, 26 (2016).
- [26] C. Shah, J. R. Crespo López-Urrutia, M. F. Gu, T. Pfeifer, J. Marques, F. Grilo, J. P. Santos, and P. Amaro, Revisiting the FeXVII line emission problem: Laboratory measurements of the $3s-2p$ and $3d-2p$ line-formation channels, *Astrophys. J.* **881**, 100 (2019).
- [27] E. Lindroth, I. Orban, S. Trotsenko, and R. Schuch, Electron-impact recombination and excitation rates for charge-state-selected highly charged Si ions, *Phys. Rev. A* **101**, 062706 (2020).
- [28] D. H. Zhang, Z. W. Wu, C. Ren, J. Jiang, L. Y. Xie, R. Schuch, J. M. Zhang, and C. Z. Dong, Calculations of Dielectronic Recombination and Electron-impact Excitation rate coefficients of highly charged sulfur ions, *Astrophys. J. Suppl. Ser.* **247**, 22 (2020).
- [29] M. F. Gu, The flexible atomic code, *Can. J. Phys.* **86**, 675 (2008).
- [30] M. S. Pindzola, N. R. Badnell, and D. C. Griffin, Validity of the independent-processes and isolated-resonance approximations for electron-ion recombination, *Phys. Rev. A* **46**, 5725 (1992).
- [31] E. Behar, P. Mandelbaum, and J. L. Schwob, Dielectronic recombination of Ne-like tungsten, *Phys. Rev. A* **59**, 2787 (1999).
- [32] N. Nakamura, Breit interaction effect on dielectronic recombination of heavy ions, *J. Phys. B: At., Mol. Opt. Phys.* **49**, 212001 (2016).
- [33] D. Bernhardt, C. Brandau, Z. Harman, C. Kozhuharov, A. Müller, W. Scheid, S. Schippers, E. W. Schmidt, D. Yu, A. N. Artemyev, I. I. Tupitsyn, S. Bohm, F. Bosch, F. J. Currell, B. Franzke, A. Gumberidze, J. Jacobi, P. H. Mokler, F. Nolden, U. Spillman, Th. Stohlker *et al.*, Breit interaction in dielectronic recombination of hydrogenlike uranium, *Phys. Rev. A* **83**, 020701(R) (2011).
- [34] D. H. Sampson, H. L. Zhang, and C. J. Fontes, A full relativistic approach for calculating atomic data for highly charged ions, *Phys. Rep.* **477**, 111 (2009).
- [35] N. R. Badnell, M. S. Pindzola, and D. C. Griffin, Validity of the independent-processes approximation for resonance structures in electron-ion scattering cross section, *Phys. Rev. A* **43**, 2250 (1991).
- [36] M. Schnell, G. Gwinner, N. R. Badnell, M. E. Bannister, S. Böhm, J. Colgan, S. Kieslich, S. D. Loch, D. Mitnik, A. Müller, M. S. Pindzola, S. Schippers, D. Schwalm, W. Shi, A. Wolf, and S.-G. Zhou, Observation of Trielectronic Recombination in Be-Like CI ions, *Phys. Rev. Lett.* **91**, 043001 (2003).
- [37] C. Beilmann, P. H. Mokler, S. Bernitt, C. H. Keitel, J. Ullrich, J. R. Crespo López-Urrutia, and Z. Harman, Prominent Higher-Order Contributions to Electronic Recombination, *Phys. Rev. Lett.* **107**, 143201 (2011).
- [38] A. Kramida, Yu.Ralchenko, J. Reader, and NIST ASD Team (2019). NIST Atomic Spectra Database (ver.5.7.1), <https://physics.nist.gov/asd>.
- [39] M. S. Pindzola, D. C. Griffin, and C. Bottcher, Resonance contributions to the electron-impact excitation of ions in the distorted-wave approximation, *Phys. Rev. A* **32**, 822 (1985).
- [40] J. Jiang, C. Z. Dong, L. Y. Xie, and J. G. Wang, Resonance electron-impact excitation and polarization of the magnetic quadrupole line of neonlike Ba^{46+} ions, *Phys. Rev. A* **78**, 022709 (2008).
- [41] J. G. Wang, T. Q. Chang, C. Z. Dong and T. Kato, Calculation of the contributions from high-n dielectronic satellites to the $K\alpha$ resonance line in helium-like iron, *Eur. Phys. J. D* **5**, 167 (1999).